Noise Analysis of MAIA System and Possible Noise Suppression

Jan ŠVIHLÍK[1], Karel FLIEGEL[2], Pavel KOTEN[3], Stanislav VÍTEK[2], Petr PÁTA[2]

[1]Dept. of Computing and Control Eng., Inst. of Chemical Tech. in Prague, Technická 5, 166 28 Prague, Czech Republic
[2]Dept. of Radioelectronics, Czech Technical University in Prague , Technická 2, 166 27 Prague, Czech Republic
[3]Interplanetary Matter Dept., Astronomical Institute of the CAS, Fričova 298, Ondřejov, Czech Republic

jan.svihlik@vscht.cz, fliegek@fel.cvut.cz

Abstract. *This paper is devoted to the noise analysis and noise suppression in a system for double station observation of the meteors now known as MAIA (Meteor Automatic Imager and Analyzer). The noise analysis is based on acquisition of testing video sequences in different light conditions and their further statistical evaluation. The main goal is to find a suitable noise model and subsequently determine if the noise is signal dependent or not. Noise and image model in the wavelet domain should be based on Gaussian mixture model (GMM) or Generalized Laplacian Model (GLM) and the model parameters should be estimated by moment method. Furthermore, noise should be modeled by GMM or GLM also in the space domain. GMM and GLM allow to model various types of probability density functions. Finally the advanced denoising algorithm using Bayesian estimator is applied and its performance is verified.*

Keywords

MAIA, meteor, noise analysis, GMM, GLM, Bayesian estimator, dicrete wavelet transform.

1. Introduction

The meteor detection and analysis is a basic topic in the field of astronomy and has a large tradition at the Astronomical Institute of the Czech Academy of Sciences of the Czech Republic.

Unfortunately, the detection of meteors is done during a night when light conditions are poor. Bad light conditions suggest noise generation in an image function or in video frames. The presence of noise in the acquired data is an unwanted event. The most of the papers are devoted to the analysis, modeling and suppression of additive noises (e.g. additive Gaussian noise). However, real imaging systems are contaminated by noise, which should be seen as additive only in special cases and only in a certain range of illumination. Several types of image noises with their models represented by probability density functions (PDF) are discussed in [1]. Gonzalez introduces Gaussian, Reyleigh, Gamma, Exponential, Uniform and Impulse noise and proposes simple pattern with several patches of constant grayscale values for imaging system testing. Hence, the basic noise parameters can be estimated directly at the patches on the acquired testing pattern by using basic statistics (sample mean, sample variance etc.). Boncelet [2] summarizes among others the noise processes (additive, multiplicative) and transforms between them.
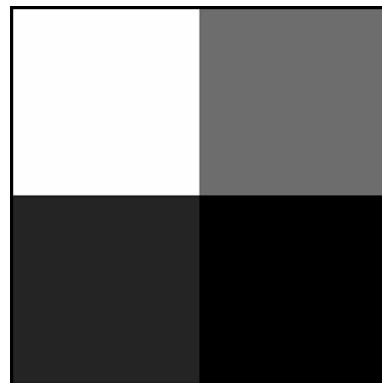

Fig. 1. Simulated testing pattern with grayscale patches equal to 31, 63, 127, 255.

A large number of imaging systems especially in astronomy contain CCD sensors [3]. A CCD sensor should be seen as a source of several noises. In the case of night sky imaging, an acquired image is contaminated by Poisson [4] noise (also known as photon counting noise) as a result of the process, where the light represented by photons is used as an information carrier. Starck [4] *et al.* also notes the so-called read out noise of CCD modeled usually as the additive Gaussian noise. Furthermore, astronomers use long exposure time because of the bad light condition during night sky acquisitions. Long exposure times suggest nonnegligible thermally generated charge called dark current. Dark current should be simply removed by a dark frame, which maps thermally generated charge in CCD. However, in the case that the dark frame is not available, the Bayesian methods should be applied. Our previous work deals with dark current analysis, modeling and suppression [13], [14].

We use the discrete wavelet transform (DWT) for im-

age representation. The DWT represents a powerful tool for image denoising, compression etc. in many application fields. Lyu and Simoncelli [5] model natural photographic images represented in multiscale basis using Gaussian Mixture Model. The authors proposed an algorithm for the additive Gaussian noise suppression on this framework. In the field of Geoscience, Amirmazlaghani [6] introduced a Bayesian-based speckle-suppression method that employed the 2-D generalized autoregressive conditional heteroscedasticity (2D-GARCH) model for wavelet coefficients of log-transformed SAR images. Nevertheless, in astronomy the wavelet based denoising plays an important role. Schmitt, Starck *et al.* [7] studied The Large Area Telescope (LAT), the main instrument of the Fermi gamma-ray Space telescope. The two main scientific objectives, the study of the Milky Way diffuse background and the detection of point sources, are complicated by lack of photons. Hence, they proposed a powerful Poisson noise removal method on the sphere which is efficient on low count Poisson data. This method uses the isotropic undecimated wavelet transform (IUWT) and the curvelet transform as spherical multi-scale transforms. The undecimated wavelet transform gives outstanding results in denoising [8].

2. Noise Analysis in Imaging Systems

Noise analysis presents a crucial procedure applied to an imaging system. The results of that analysis allow to propose an advanced denoising algorithm for noise suppression. The noise analysis should be based on acquisition of a testing pattern, which contains several patches with constant greyscale levels from white to black [1]. In the simplest case, a pattern for the measurement of transfer function should be used. The example of the simulated testing pattern along with its histogram can be seen in Fig. 1 and Fig. 2. If we consider contamination of the pattern by additive gaussian noise, the histogram is changed in accordance with Fig. 2 b). This figure illustrates that the noise parameters are independent of the signal value. Furthermore, the parameters of the Gaussian noise should be simply estimated from the testing pattern using basic statistics. There is a histogram of the simulated testing pattern contaminated by Poisson noise (also known as photon counting noise) in Fig. 2 c).

2.1 Data Acquisition in Current System

Current system for meteor observation consists of object lens Jupiter 2/85 mm or eventually Arsat 1.4/50 mm, image intensifier of the second generation Mullard XX1332 and S-VHS camera Panasonic. The video from the camera is saved on a magnetic tape and then digitized in the following way: 768x576 pixels, 25 frames per second, 256 grayscale levels, non-compressed.

Since the system for meteor observation is installed at Astronomical Institute, the testing of the system was done by acquisition of so-called flat field video sequences. The flat
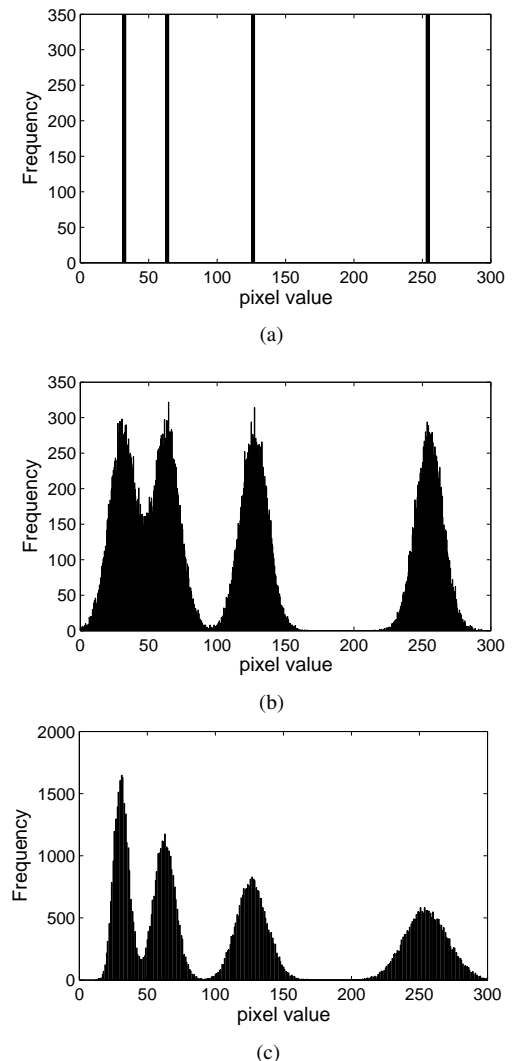

Fig. 2. a) Histogram of the simulated testing pattern, b) Histogram of the pattern contaminated by additive Gaussian noise with σ = 10, c) Histogram of the pattern contaminated by Poisson noise.

field video sequences are given by acquisition of the area with approximately constant grayscale level (acquisition of the sky through a paper after sunset). The time after sunset was set to 7, 18, 28, 32 minutes to simulate the area with constant greyscale level. However, the acquired frames also map the non-uniform illumination of the system. Hence we create the so-called master field from certain frames from several video sequences. Master field frames are computed simply by averaging all frames from sequences to suppress the analyzed time variant noise. The example of the master field frame is depicted in Fig. 3. Hence now it is possible to eliminate the non-uniform illumination in all video frames by subtraction the master flat field from the frames to be analyzed. Now we have the video frames suitable for further noise analysis.

2.2 Noise Analysis in Current System

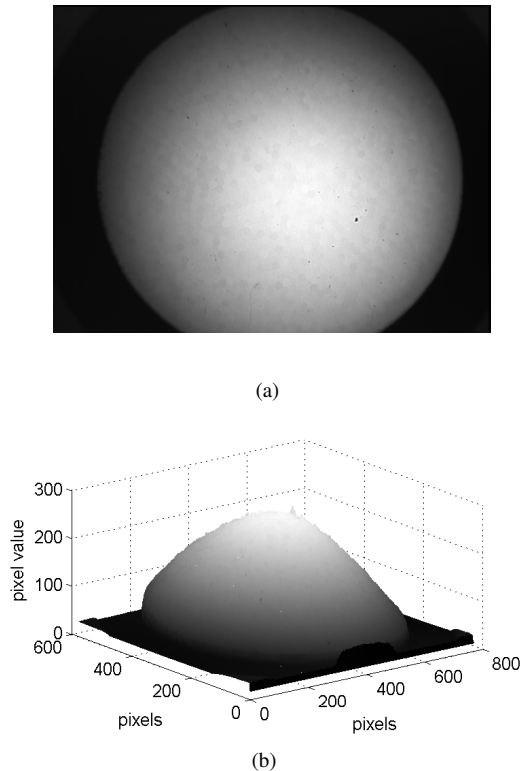As mentioned above, all frames from several video sequences are corrected by the master field frame. Hence we

(a)

(b)

Fig. 3. Master flat field created by using the video sequences acquired 7 minutes after sunset.

have frames with eliminated non-uniform illumination of the observation system. Firstly we evaluate an optimized histogram of the corrected frames to find the noise PDF. The quality of the histogram shape depends mainly on its bin width. There are many approaches to the bin width B_W optimization, e.g. [12] and [11]. In [12] it has been shown that the optimal histogram bin size, which provides the most efficient unbiased estimation of the PDF, is given by

$$B_W = 3.49 \sigma I^{-\frac{1}{3}} \qquad (1)$$

where B_W is the bin width of the histogram, σ denotes the standard deviation of the distribution, I presents the number of samples. A similar, but more robust, result was obtained by Freedman and Diaconis (summarized in [11]). Their bin width can be written as

$$B_W = 2(x_{0.75} - x_{0.25})I^{-\frac{1}{3}} \qquad (2)$$

where the term in the parentheses denotes so-called interquartile range, $x_{0.75}$ is the 75th percentile and $x_{0.25}$ is the 25th percentile.

Fig. 4 a) and b) show the optimized histograms of the chosen area (in the center of the frame, 320x320 pixels) in the frames at all times after sunset along with the sample variances $D(n) = \frac{1}{I-1} \sum_{i=1}^{I} (n_i - E(n))^2$ of noise n with subtracted mean value $E(n) = \frac{1}{I} \sum_{i=1}^{I} n_i$. The dependency of $D(n)$ on the maximum values of the master flat field is depicted in Fig. 6. Histograms are similar to Gaussian PDF.

We applied Kolmogorov-Smirnov test, the null hypothesis (samples come from Gaussian distribution) at significance level $\alpha = 0.05$ was rejected. Hence it is necessary to model the noise by using a more general model.

We choose the model for heavy-tailed noise based on exponential. The PDF of heavy-tailed noise is given by

$$p_n(n; \mu, s, \nu) = \frac{e^{-\left|\frac{n-\mu}{s}\right|^\nu}}{Z(s, \nu)}, \qquad n \in (-\infty; \infty) \qquad (3)$$

where μ denotes the mean value, parameter ν presents generalization in the sense of the shape of the heavy tailed PDF and the parameter s controls the width of the PDF. The function $Z(s, \nu) = \frac{2s}{\nu} \Gamma\left(\frac{1}{\nu}\right)$, where $\Gamma(x) = \int_0^\infty t^{x-1} e^{-t} dt$, normalizes the exponential to a unit area. The parameters of PDF given by (3) should be estimated simply by using the system of moment equations [9]. For simplicity we consider noise n with $\mu = 0$, the second and fourth moment runs as

$$m_2(s, \nu) = \frac{s^2 \Gamma\left(\frac{3}{\nu}\right)}{\Gamma\left(\frac{1}{\nu}\right)}, \qquad m_4(s, \nu) = \frac{s^4 \Gamma\left(\frac{5}{\nu}\right)}{\Gamma\left(\frac{1}{\nu}\right)}. \qquad (4)$$

In accordance with [9], the parameters estimation should be simplified using kurtosis

$$\kappa_n = \frac{m_4(s, \nu)}{m_2^2(s, \nu)} = \frac{\Gamma\left(\frac{5}{\nu}\right) \Gamma\left(\frac{1}{\nu}\right)}{\Gamma^2\left(\frac{3}{\nu}\right)}. \qquad (5)$$

The above mentioned model is well known as the Generalized Laplacian Model (GLM) and it is usually used to model filtered images (e.g. wavelet coefficients of high frequency bands). Fig. 4 c) and d) show that the models fit the optimized histograms well. All models are plotted in the logarithmic domain, because the quality of the fit is clearly visible. The fits are satisfactory also in the sense of Jeffrey divergence [10] (a measure of the distribution similarity), (6):

$$J_D = \sum_{i=1}^{I} \left[p_i^a \ln\left(\frac{p_i^a}{0.5(p_i^a + p_i^b)}\right) + p_i^b \ln\left(\frac{p_i^b}{0.5(p_i^a + p_i^b)}\right) \right] \qquad (6)$$

where I stands for the number of PDF samples, p^a denotes the model PDF and p^b presents the normalized histogram of the dark frame.

2.3 Data Acquisition in New System

The new system for meteor observation is in its basic design similar to the above described analog system which is still in use at the Astronomical Institute. The new system consists of fast lens Pentax SMC FA 1.4/50 mm, image intensifier of the second generation Philips (Photonis) XX1332 and progressive scan monochrome camera JAI CM-040GE with GigE Vision interface equipped with fast lens Pentax H1214-M 1.4/12 mm. The camera in the test setup in Fig. 5 was delivering an uncompressed video stream of 61.15 frames per second with resolution of 776x582 pixels and 256 greyscale levels. The shutter was set to 1/100 s exposure time.
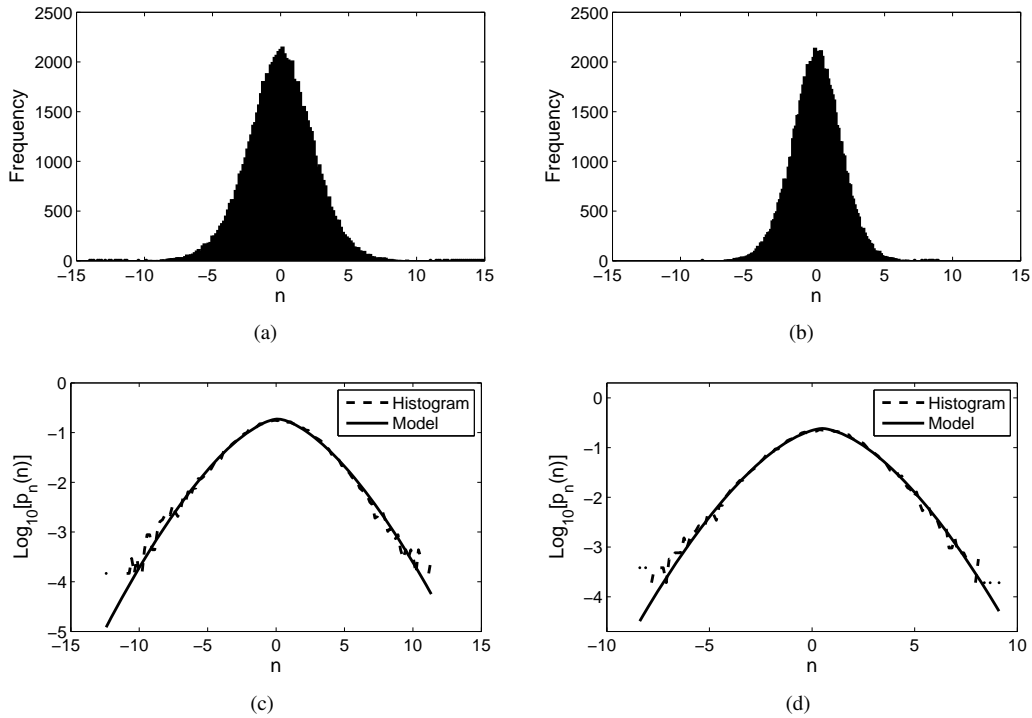
(a)

(b)

(c)

(d)

Fig. 4. Histograms of the chosen area of the flat fielded frames at particular times after sunset, subtracted mean value $E(n)$, a) 7 minutes, $E(n) = 0.12$, $D(n) = 6.13$, b) 32 minutes, $E(n) = 0.47$, $D(n) = 3.39$ and normalized histograms along with the models, c) 7 minutes, $\nu = 1.57$, $s = 3.04$, $J_D = 0.0062$, d) 32 minutes, $\nu = 1.62$, $s = 2.30$, $J_D = 0.0081$.
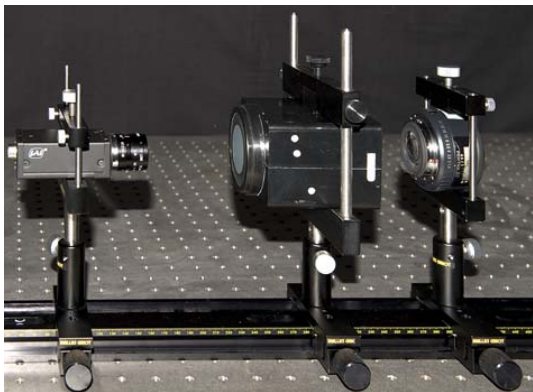

Fig. 5. Test setup.

The system was installed on a test bed in optical laboratory thus the test video could be captured in well controlled conditions. The testing has been done in similar manner as in the case of current analog system as described above. The flat field video sequences of the area with approximately constant luminance level were captured. The captured scene was made of a whitepaper screen evenly illuminated with LOT-Oriel halogen light source. The broadband light beam of the halogen lamp was filtered with Carl Zeiss interference filter into the narrowband around 650 nm wavelength where the peak sensitivity of the XX1332 image intensifier is. The average luminance of the screen was maintained constant while capturing a set of 100 frames for each luminance level. The luminance was controlled with a stabilized LOT-Oriel power supply and checked with the NIST certified radiometric light meter system.

Video frames acquired as described above contain obvious non-uniformity in the brightness level which is not desirable for the noise analysis. To solve this problem the same approach in data preprocessing was applied as in the case of the current analog system. The master field was calculated from 100 frames in the videosequence acquired at the same average luminance level. This master field in the particular test sequence is again simply an average of all 100 frames in this sequence. Then the non-uniform illumination in all video frames was eliminated by subtraction of the master flat fields from the frames in each test sequence. Noise analysis was then conducted in the same way as for the current analog system.

2.4 Noise Analysis in New System

We optimized noise analysis in the new system to be comparable with the analysis in current system. Hence, the procedure of analysis was similar as in the case of current system still installed at the Astronomical Institute. Firstly, the master flat fields were created from the acquired video sequences and all frames in each sequence were corrected. The optimized histograms estimated from corrected video frames have shown that the noise should again be modeled by GLM given by (3). The chosen histograms with the nearest maximum flat field values (see Tab. 1) as in the measurement of current system are depicted in Fig. 7 a) and b). The dependency of $D(n)$ on the maximum values of the master flat field is depicted in Fig. 6.

Figure 5. and 9.	a)	b)	c)	d)
maximum value of flat field, current system	253	233	195	130
maximum value of flat field, new system	251	234	191	135

Tab. 1. The maximum values of master flat fields for the current and new system.
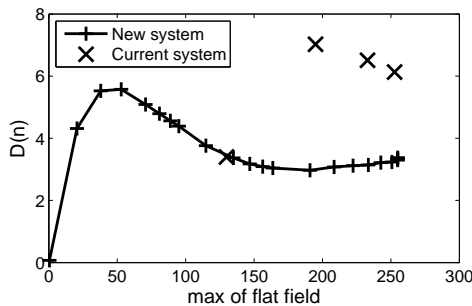

Fig. 6. Dependency of variance $D(n)$ on the maximum value of master flat fields of the current and new system.

3. Proposed Denoising Algorithm

Nowadays, we have the first image data of night sky from the new system. The new system is just installed. Hence, we tested the proposed denoising algorithm on the acquired testing video sequences. Previous chapters show that noise should be modeled by one dimensional model called GLM. This suggests an utilization of Bayesian estimator (MMSE or MAP) for the estimation of the denoised image function. Furthermore, an image function presented by video frame should be modeled also by GLM. Hence, it is suitable to apply Discrete Wavelet Transform to the acquired data.

3.1 Discrete Wavelet Transform

In the case of an image denoising, the undecimated wavelet transform (UWT) is better to be used. The undecimated transform produces the same number of wavelet coefficients at each scale and it is also called Stationary Wavelet Transform (SWT). SWT is computed using so-called à trous algorithm [17]. The decimated wavelet transform [16] is shift variant. This characteristic limits the denoising performance [15].

There is a basic structure for the decimated wavelet transform called dyadic decomposition shown in Fig. 8. Here, Hi and Lo present the impulse response of the high pass filter and the low pass filter respectively, $2\downarrow$ denotes down sample by the factor of 2. If the signal is filtered using the scheme in Fig. 8 then four subbands (matrices) are obtained, i.e. diagonal details (HH) $\gamma D_{p+1}^{(d)}$, vertical details (HL) $\gamma D_{p+1}^{(v)}$, horizontal details (LH) $\gamma D_{p+1}^{(h)}$ and signal approximation (LL) γA_0. The matrix γA_0 presents the signal which is to be decomposed.

We utilized both transforms, the decimated and undecimated one. The image data were decomposed up to the

5th decomposition level using the filters derived from the wavelet Daubechies6.

An important task in image processing while using wavelet transform is to chose a suitable wavelet [15]. Firstly, it is known that image denoising becomes simpler in a sparse wavelet representation (i.e. only a small number of wavelet coefficients with large magnitude). This statement [15] holds mainly for decimated wavelet transform (e.g. dyadic decomposition). Secondly, it is necessary to pay attention to the image quality. Thus, the goal is to produce as many wavelet coefficients that are close to zero as possible. This depends on the vanishing moments N_v and on the support size K of the analysis wavelet. For the image quality, the regularity and symmetry of the synthesis wavelet are important. In the orthogonal case, it is difficult to achieve a large number of vanishing moments and a small support size at the same time. The theoretical limit is $K = 2N_v - 1$ and is achieved in the Daubechies wavelets, usually denoted as dbN_v.

We optimized the mother wavelet in the sense of RMSE (Root Mean Square Error) (13). We minimize the RMSE between original image x and the denoised image $\widehat{x}$. The process of optimization is given by

$$\widehat{h} = \underset{h=[h_1,\dots h_k]}{\arg\min} \mathcal{RMSE}(x,\widehat{x}) \qquad (7)$$

where $\widehat{h} = [h_1,\dots h_k]$ denotes the optimal decomposition filter derived from the mother wavelet. We tested the orthogonal and compactly supported wavelets: Daubechies (Db1-Db10), Symlet (Sym2-Sym8) and Coiflet (Coif1-Coif5). The optimization was done numerically using our testing data. However, the results of optimization showed that all tested wavelets give practically the same results. Only the results of optimization of the shortest filters (e.g. derived from Haar wavelet) were considerably worse as it should be assumed.

3.2 MMSE (Minimum Mean Square Error)

For the simplicity, the additive noise is assumed $y = x + n$, where y denotes the noisy observation (acquired data), n presents noise and x is a clean image function. The conditional mean of the posterior PDF provides a least square estimation of x. MMSE [9] estimator runs as

$$\hat{X}(Y) = \frac{\int_{-\infty}^{+\infty} p_N(y-x) p_X(x) x \, dx}{\int_{-\infty}^{+\infty} p_N(y-x) p_X(x) \, dx}. \qquad (8)$$

The capital letters in (8) mean the wavelet domain. The MMSE estimator is applied on all detailed wavelet bands up to the 5th decomposition level, whereas the image parameters are estimated using the system of the moment equations. The denoised image is obtained by inverse wavelet transform applied on the modified detailed wavelet bands.

3.3 Method of Moments

Similarly as in [13], we define the theoretic central moments of Y. The second moment m_2 of Y is given by addition
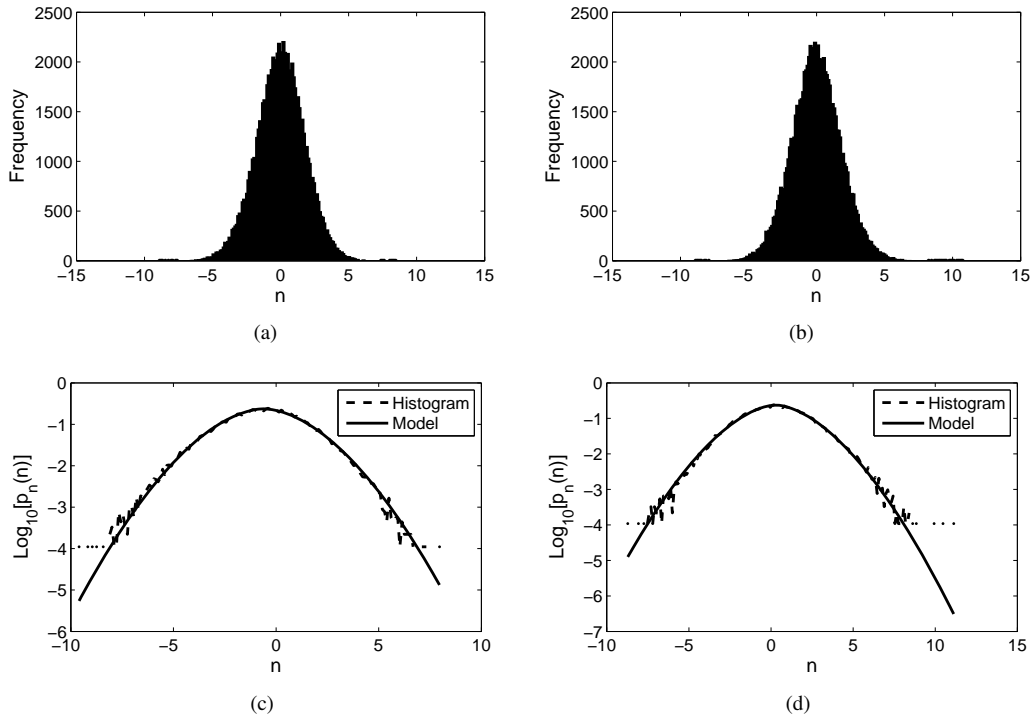
Fig. 7. Histograms of the chosen area of the flat fielded frames with the nearest maximum flat field value as in the measurement of current system, subtracted mean value $E(n)$, a) $E(n) = -0.60$, $D(n) = 3.23$, b) $E(n) = 0.28$, $D(n) = 3.37$ and normalized histograms along with the models, c) $\nu = 1.78$, $s = 2.38$, $J_D = 0.0113$, d) $\nu = 1.71$, $s = 2.36$, $J_D = 0.0101$

of several GLM moments

$$m_2(Y) = \frac{\delta^2 \Gamma\left(\frac{3}{\varepsilon}\right)}{\Gamma\left(\frac{1}{\varepsilon}\right)} + \frac{s^2 \Gamma\left(\frac{3}{\nu}\right)}{\Gamma\left(\frac{1}{\nu}\right)} = m_2(X) + m_2(N) \quad (9)$$

where δ and ε are the GLM parameters of the signal. The fourth moment m_4 of Y runs as

$$
\begin{aligned}
m_4(Y) &= \frac{\delta^4 \Gamma\left(\frac{5}{\varepsilon}\right)}{\Gamma\left(\frac{1}{\varepsilon}\right)} + \frac{6s^2\delta^2 \Gamma\left(\frac{3}{\nu}\right)\Gamma\left(\frac{3}{\varepsilon}\right)}{\Gamma\left(\frac{1}{\nu}\right)} + \frac{s^4 \Gamma\left(\frac{5}{\nu}\right)}{\Gamma\left(\frac{1}{\nu}\right)} \\
&= m_4(X) + 6m_2(N)m_2(X) + m_4(N). \quad (10)
\end{aligned}
$$

The parameters of the signal GLM will be estimated using kurtosis

$$
\begin{aligned}
\kappa_X &= \frac{\Gamma\left(\frac{5}{\varepsilon}\right)\Gamma\left(\frac{1}{\varepsilon}\right)}{\Gamma^2\left(\frac{3}{\varepsilon}\right)} \quad (11) \\
&= \frac{m_4(Y) - m_4(N) - 6m_2(N)(m_2(Y) - m_2(N))}{(m_2(Y) - m_2(N))^2}
\end{aligned}
$$

From (9) we should derive

$$\delta = \sqrt{(m_2(Y) - m_2(N))\frac{\Gamma\left(\frac{1}{\varepsilon}\right)}{\Gamma\left(\frac{3}{\varepsilon}\right)}}. \quad (12)$$

The values of the moments should be estimated from the data using the sample moments. The kth central sample moments of X is given by $M_k(X) = \frac{1}{I}\sum_{i=1}^{I}(X_i - E(X))^k$.

3.4 Results

There will be presented the results obtained by denoising algorithm based on Bayesian estimator and GLM
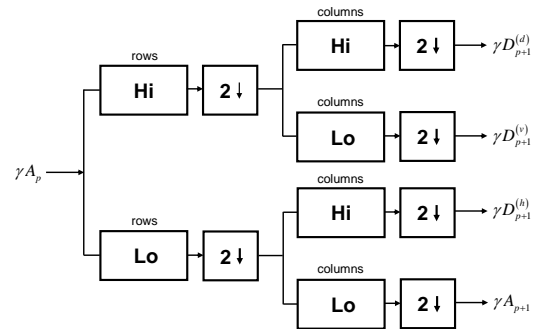

Fig. 8. Implementation of 2-D dyadic decomposition.

model for the noise and image function. Two implementations of the discrete wavelet transform were applied: UWT and DWT. The noise characteristics were found by measurement and statistical analysis. Tab. 2 contains the obtained RMSE, where *RMSEi* (should be seen as a standard deviation of the noise) denotes the error computed between the noisy flat field and the master flat field. The denoising performace is illustrated by the values of *RMSEo* evaluated between master flat field and the denoised flat field. The *RMSE* is given by

$$RMSE = \sqrt{\frac{1}{I}\sum_{i=1}^{I}(x - \hat{x})^2} \quad (13)$$

where x denotes the original image and $\hat{x}$ is the denoised image. The first row of Tab. 2 ROFF denotes range of flat field values. The chosen denoised images and the corresponding noisy images are depicted in Fig. 9.
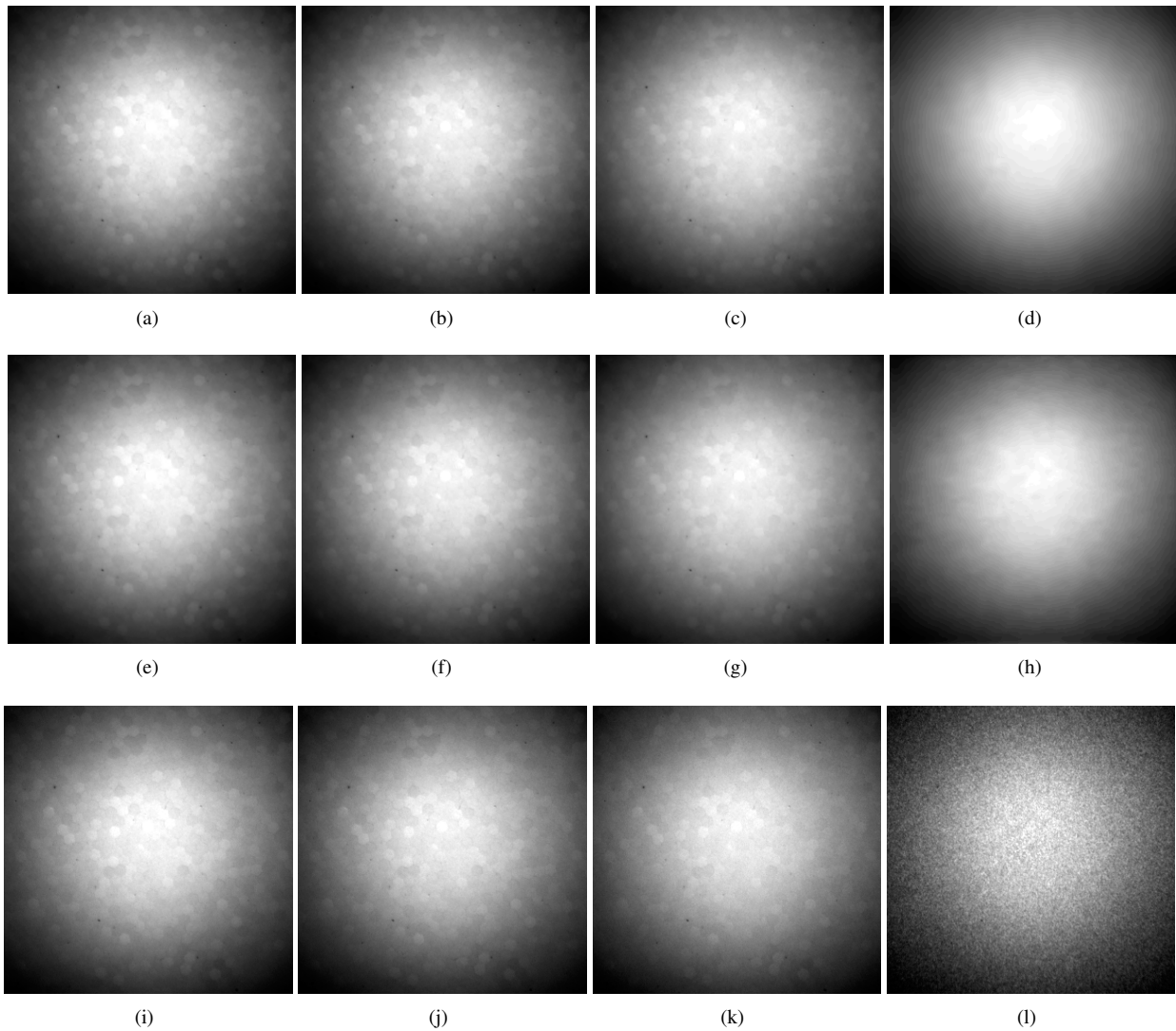
Fig. 9. Flat fields denoised using DWT a)-d), using UWT e)-h) acquired at certain light conditions and the noisy flat fields i)-l), i) ROFF 23-255, j) ROFF 22-251, k) ROFF 19-191, l) ROFF 5-53.

ROFF	RMSEi	UWT: RMSEo	DWT: RMSEo
23-255	1.89	1.29	1.33
22-251	1.82	1.17	1.22
19-191	1.67	0.93	0.97
12-115	1.87	0.84	0.82
5-53	2.26	0.60	0.52
2-21	1.99	0.36	0.31

Tab. 2. The summary of RMSE.

4. Conclusion

Two systems for the detection of meteors were tested. The current system was measured at four time instants after sunset and the measurement of the new system was done in a wide range of illumination. After that, the four nearest measuring points in the sense of maximum value of master flat field were found in the results of the measurement of the new system.

The estimated values of shape parameters ν of GLM are approximately 1.7 for the new system and approximately 1.5 for the current system. These parameter values suggest that the central limiting theorem was not well satisfied. This means that the generated noise is more general (in the sense of the parameter ν) than the Gaussian random variable. The GLM model was used instead of GMM for simplicity.

The dependency of the variance of maximum values of the master flat field in Fig. 6 shows that the variance of the new system changes slightly in a certain range. Unfortunately, the new system will probably be operating at very low illumination, where the generating noise will be signal dependent.

An algorithm for image denoising was proposed. Since we modeled both signals (image and noise) by the GLM model in the wavelet domain, we are able to denoise video frames contaminated by noise with variable shape of its PDF. Furthermore, a specific hexagonal mosaic in the images is

given by the channels on micro channel plate of image intensifier.

References

[1] GONZALEZ, R. C., WOODS, R. E *Digital Image Processing.* 2nd Ed. Upper Saddle River (USA): Prentice Hall, 2002.

[2] BONCELET, C. Image noise models. BOVIK, A. (Ed.) *Handbook of Image and Video Processing.* 2nd ed. Elsevier, 2005.

[3] BUIL, C. *CCD Astronomy: Construction and Use of an Astronomical CCD Camera.* Richmond (USA): Willmann-Bell, 1991.

[4] STARCK, J. L., MURTAGH, F., BIJAOUI, A. *Image Processing and Data Analysis: The Multiscale Approach.* Cambridge University Presss, 1998.

[5] LYU, S. W., SIMONCELLI, E. P. Modeling multiscale subbands of photographic images with fields of gaussian scale mixtures. *IEEE Trans. on Pattern Anal. and Mach. Intell.*, 2009, vol. 31, no. 4, p. 693 - 706.

[6] AMIRMAZLAGHANI, M., AMINDAVAR, H. Two novel bayesian multiscale approaches for speckle suppression in SAR images. *IEEE Transactions on Geoscience and Remote Sensing*, 2010, vol. 48, no. 7, p. 2980 - 2993.

[7] SCHMITT, J., STARCK, J. L. *et al.* Poisson denoising on the sphere: application to the Fermi gamma ray space telescope. *Astronomy and Astrophysics*, 2010, vol. 517, no. A26.

[8] RAPHAN, M., SIMONCELLI, E. P. Optimal denoising in redundant representations. *IEEE Transactions on Image Processing*, 2008, vol. 17, no. 8, p. 1342 - 1352.

[9] SIMONCELLI, E. P. Noise removal via Bayesian wavelet coring. In *Proceedings of 3rd IEEE International Conference on Image Processing.* Lausanne (Switzerland), 1996, p. 379 - 382.

[10] SMITH, P. *et al.* Effective corner matching. In *Proc. of the Ninth BMVC 98,* Cambridge: Massachusetts Inst. of Technology, 1998.

[11] IZENMAN, A. J. Recent developments in nonparametric density estimation. *J. of the Amer. Stat. Assoc.*, 1991, vol. 86, no. 413, p. 205 - 224.

[12] SCOTT, D. W. On optimal and data-based histograms. *Biometrika*, 1979, vol. 66, no. 3, p. 605 - 610.

[13] ŠVIHLÍK, J., PÁTA, P. Elimination of thermally generated charge in charged coupled devices using Bayesian estimator. *Radioengineering*, 2008, vol. 17, no. 2, p. 119 - 124.

[14] ŠVIHLÍK, J. Modeling of scientific images using GMM. *Radioengineering*, 2009, vol. 18, no. 4, p. 579 - 586.

[15] PIZURICA, A. *Image Denoising using Wavelets and Spatial Context Modeling.* Ph.D. dissertation. Gent (Belgium): Univ. Gent, 2002.

[16] MALLAT, S. G. A theory for multiresolution signal decomposition: the wavelet representation. *IEEE Trans. on Pattern Anal. and Mach. Intell.*, 1989, vol. 2, no. 7, p. 674 - 693.

[17] HOLSCHNEIDER, M., KRONLAND-MARTINET, R., MORLET, J., TCHAMITCHIAN, P. A real time algorithm for signal analysis with the help of the wavelet transform. COMBES, J.-M., GROSSMANN, A., THAMITCHIAN, P. (Eds.) *Wavelets: Time-Frequency Methods and Phase Space.* Berlin: Springer, 1989.

About Authors...

Jan ŠVIHLÍK was born in Pardubice, Czech Republic, in 1981. He received his M.Sc. (Ing.) from the Czech Technical University in Prague (CTU), in 2005 and Ph.D. from the CTU, in 2008. Now he is an assistant professor at the Institute of Chemical Technology Prague. His research interests include image processing, image denoising, astronomical images and statistical models of images.

Karel FLIEGEL was born in Prague, Czech Republic, in 1979. He received his M.Sc. degree in electrical engineering from the Czech Technical University in Prague (CTU) in 2004. Now he is an assistant professor at the CTU and he is finishing his Ph.D. His research interests include image processing, imaging systems, image and video compression.